AN ANALYSIS OF ZERO DEGREE CALORIMETER SHOWER MAXIMUM DETECTOR DATA FOR POLARIMETRY AT STAR

JOSHUA N. KELLAMS

A THESIS SUBMITTED IN PARTIAL FULFILLMENT OF THE REQUIREMENT FOR THE DEGREE OF

MASTER OF SCIENCE

BALL STATE UNIVERSITY

DR. DAVID GROSNICK

JULY 12, 2010

Table of contents

List of Figures

List of Tables

Abstract

The Zero Degree Calorimeter at STAR was used to calculate an asymmetry from small-angle scattering of neutral particles from proton-proton collisions at a center-of-mass energy of 500 GeV. An energy-centroid method was used to define hit positions of the neutral particles for each Shower Maximum Detector plane. An angular asymmetry analysis was done using these positions to measure both a left-right and a top-bottom asymmetry. The asymmetries were then used to calculate transversely-normal and sideways beam-polarization components for both of RHIC's polarized-proton beams. The results of this analysis show that the Zero Degree Calorimeter Shower Maximum Detectors can be used as effective polarimeters at high beam energies, and can check the functionality of the spin rotators for longitudinally-polarized beams. The results of this analysis will be used in measurements that further the understanding of the source of a proton's spin.

Chapter I

Introduction

The exact source of a proton's spin is unknown. A proton's spin may contain contributions from its constituents, quarks and gluons, and the angular momentum of these constituents. Experiments [1-3] are currently taking place to measure these contributions; for example, the spin measurements made at STAR, PHENIX, and HERMES. Each of these experiments uses a detector, which measures an interaction asymmetry, and a polarized beam, which fixes the spin direction of the particles. In order for these experiments to be viable, the polarization of the beam particles involved in the interaction must be known.

The Relativistic Heavy Ion Collider (RHIC), located at Brookhaven National Laboratory, is a facility capable of accelerating heavy ions and polarized protons. The focus of the RHIC spin physics program is to gain a better understanding of the spin structure of the proton using polarized-proton beams. Information from each spin contributor is incomplete; some of this information will be provided by polarized-proton data taken with the Solenoidal Tracker at RHIC (STAR). STAR is a large detector system whose primary design is to study heavy-ion collisions, but can also be used to investigate polarized proton-proton collisions [4]. To be able to use these data, the beam polarization must be known locally at the STAR detector.

Currently, the local beam-polarization measurement at STAR is made by two scintillator arrays [5], located 3.75 meters on either side of the collision point. At higher

beam energies, this may be an insufficient polarization measurement. Particles produced in high-energy collisions are relativistically-boosted forward and may scatter at small angles with trajectories that miss the arrays currently being used as polarimeters. The effect due to the physics processes, called the analyzing power, measured in these arrays may also be diminished at higher energies, thus limiting their effectiveness as a polarimeter. For these higher beam energies, detectors placed much further from the collision point can be used to measure a neutral particle asymmetry from small-angle scattering, as given in reference [6]. An analysis of this neutral particle asymmetry can provide the analyzing power for the small-angle scattering measured in the detectors far from the collision point. The analyzing power, in turn, leads to a measurement of the local beam polarization.

This thesis reports on a method to measure the local beam polarization at STAR. Chapter II contains information on the experimental facility and the detectors. Chapter III describes the data analysis, which includes the sample data sets used, corrections to the raw data, the method used to categorize the data, and the calculations that were performed. Some specific information concerning the data and analysis described in Chapter III are located in the appendices. Chapter IV contains the results of the analysis, the conclusions of those results, as well as possibly beneficial future analyses of the data.

Chapter II

Detector

The Relativistic Heavy Ion Collider is the only facility in the world capable of accelerating beams of high-energy polarized protons and colliding them head-on. The RHIC facility is shown in Fig. 1. Polarized protons used in the high-energy collisions begin with an atomically-polarized ion source. These polarized protons are accelerated by a linear accelerator to an energy of 200 MeV, at which time they are injected into the booster ring, that increases the energy to 1.5 GeV. Next, they proceed into the Alternating Gradient Synchrotron (AGS), where the protons are accelerated to 25 GeV. After the AGS, the beam is then split into two separate beams (labeled "yellow" and "blue") before they are injected into the RHIC storage ring [7], where each beam energy is increased up to 250 GeV. The blue beam travels around the ring clockwise in one pipe, while the yellow beam travels counterclockwise in another. The two beams cross paths at collision points that are located at several places around the ring; refer to Fig. 1.

Polarization measurements are taken by two types of Coulomb-nuclear interference (CNI) polarimeters [8] that provide an absolute beam polarization. One type uses four polarimeters, two in each beam, involving elastic proton-carbon scattering and the other type involves scattering of beam protons on a hydrogen jet target. The positions of the three CNI polarimeters can be seen in Fig. 1.

The STAR detector [4] consists of numerous sub-detectors with the overall function to measure particle production over a large solid angle, as shown in Fig. 2. The

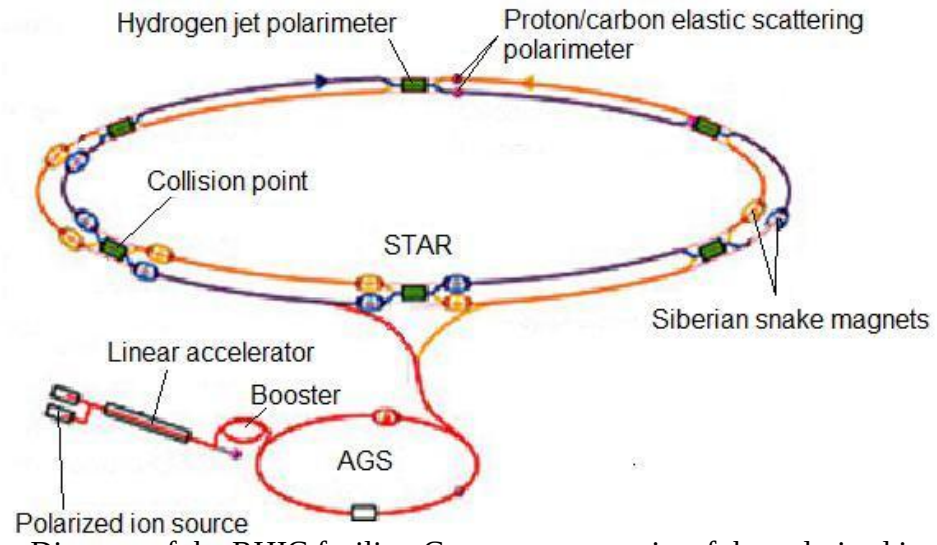

Fig. 1: Diagram of the RHIC facility. Components consist of the polarized ion source, linear accelerator, booster ring, Alternating Gradient Synchrotron (AGS), and the large RHIC storage ring. Positions of polarimeters, Siberian snake magnets, and the STAR detector are shown [7].

principal sub-detector within STAR is a large Time Projection Chamber (TPC) that is used for charged-particle identification and tracking. In addition, STAR consists of a large solenoid magnet for momentum analysis, a Barrel Electromagnetic Calorimeter (BEMC) that provides energy information from particles after a collision, and many other specialized detectors. Two detectors that are not part of the main STAR detector, called the Zero Degree Calorimeters (ZDCs) [9], are used with STAR to measure event geometry for heavy-ion collisions. A study [6] was performed to show the potential of using the ZDC SMDs as a polarimeter for beams with center of mass energy of 200 GeV. The results of that study showed that it is possible to use the ZDC SMDs as a local polarimeter at STAR.

For the RHIC accelerator, the stable spin configuration of polarized-proton beams is vertical, labeled as transversely-normal, which means perpendicular to the beam-

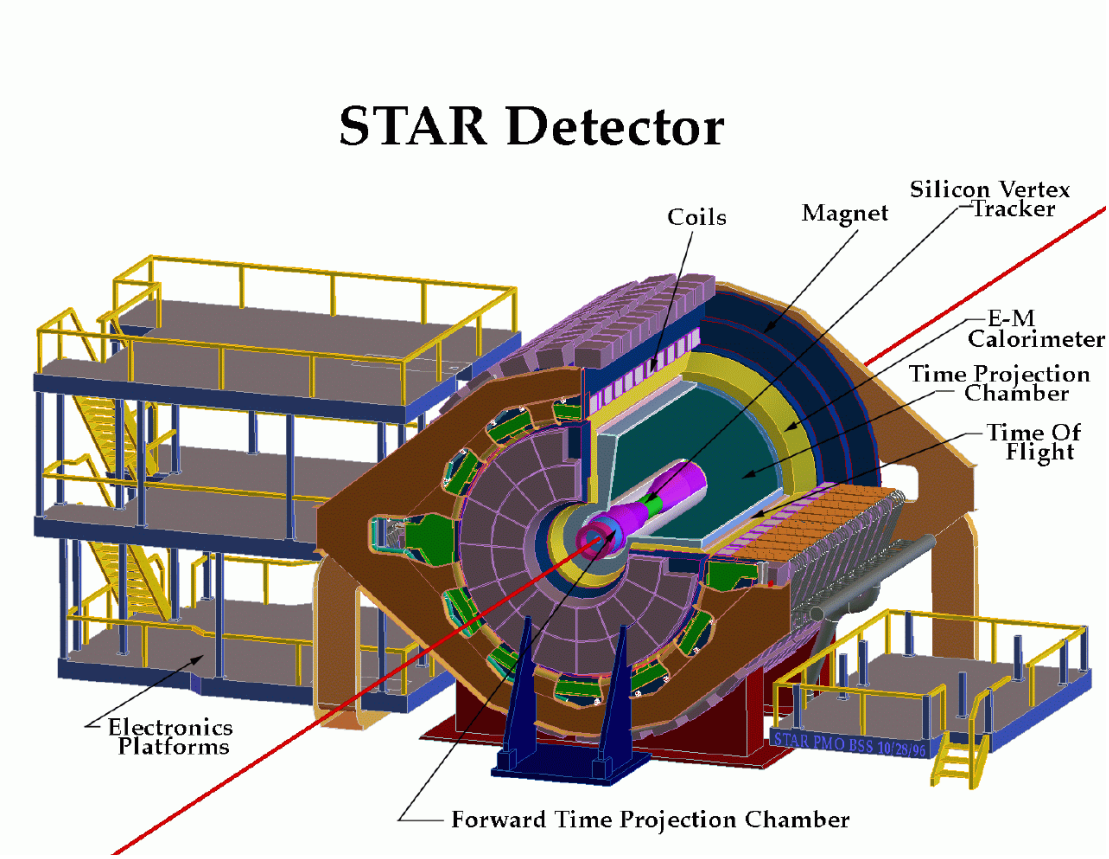

Fig. 2: Diagram of the Solenoid Tracker at RHIC (STAR). The location of various components, such as the magnet, Time Projection Chamber (TPC), Barrel Electromagnetic Calorimeter (BEMC), labeled as E-M Calorimeter, and other sub-detectors, are shown [4].

particle momentum. Small imperfections in the bending magnets and depolarizing resonances can cause slight changes to the stable polarization orientation, and consequently, a depolarization of the proton beam. In order to stop this depolarization effect, two helical, dipole magnets, called Siberian snakes [7], were placed in each beam line, as shown in Fig. 1. The goal of the Siberian snakes is to rotate the spin orientation of each proton 180 degrees without affecting the trajectory of the beam. This 180 degree flip causes any depolarization effect that each proton may encounter during one orbit

around the RHIC ring to be undone on the next orbit. If the Siberian snakes were not present, a proton beam orbiting the ring would be depolarized a little more on each orbit, ultimately resulting in a complete depolarization of the beam [10-12].

To study spin interactions using polarized protons with different spin orientations, RHIC needs to have the ability to collide protons of a given orientation with a proton of any other spin orientation that may be required for physics measurements. For this spin-orientation control, RHIC uses half-length Siberian Snake magnets, called spin rotators [13, 14]. A spin rotator for each beam is located on both the east and west sides of the STAR detector; see Fig. 1. After the collision, any remaining protons in the beam are rotated back to the stable transversely-normal orientation using a second spin rotator for that beam. The use of spin rotators around the STAR collision point makes it necessary to check the local polarization of each beam.

Two detectors far upstream and downstream of the STAR collision point, called the Zero Degree Calorimeters (ZDC), were originally designed to detect and measure the energy of neutral particles emitted within 2 milliradians from the axis of the beam from heavy-ion collisions. In these heavy-ion collisions, the measurements [9] are used to determine the event geometry, as well as beam luminosity. Any charged particles that are produced in these interactions are swept away along the beam line by bending magnets that are just upstream of the ZDCs. Therefore, neutral particles account for nearly the entire total energy found in the ZDCs, while charged particles contribute only negligible amounts [9]. It has been estimated [15] that the neutral particles are mostly neutrons with small numbers of antineutrons, K_L^0 particles and photons.

As shown in Fig. 3, each ZDC detector is located 18 meters from the intersection point of the two beams on both sides of STAR and is placed between the blue and yellow beam lines. Each ZDC detector consists of 3 identical calorimeter modules, as well as a set of scintillator planes, called a Shower Maximum Detector (SMD); see Fig. 4. All modules in the ZDC are tilted at 45 degrees relative to the beam direction in order to optimize the sensitivity to charged particles produced in hadronic showers from neutral particle interactions [9]. The 45 degree tilt of the modules is primarily used for heavy-ion collisions.

An SMD [6] is used to provide position information from neutral particle showers, and is located between ZDC modules 1 and ZDC modules 2, as shown in Fig. 4. The construction of the SMDs consists of 32 horizontal strips and 21 vertical strips, with each set forming a plane. Each strip is a scintillator with a triangular cross section (see Fig. 5) and is wrapped in aluminized Mylar to prevent leakage of light, produced during the scintillation process, to its neighboring strips. Adjacent strips are fitted with one facing up and the next facing down forming a plane, as shown in Fig. 5. Through the center of

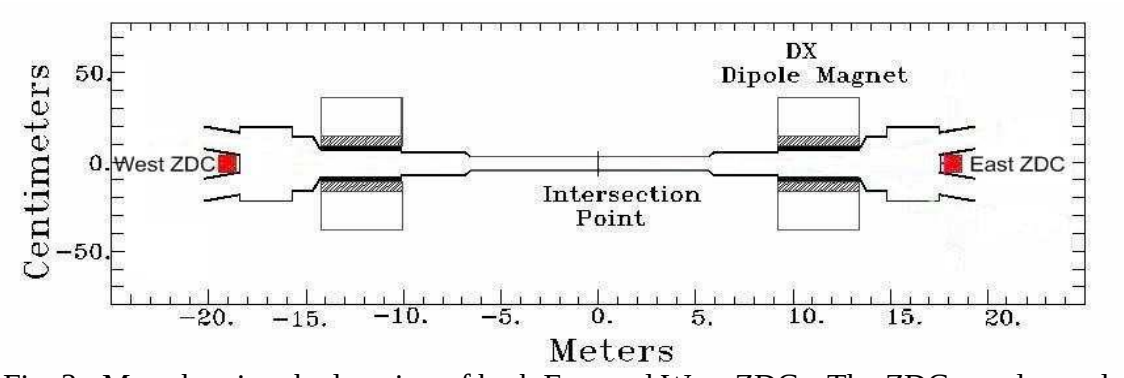

Fig. 3: Map showing the location of both East and West ZDCs. The ZDCs are located between the beam lines after the bending magnets. Note the large difference in distance scales between the *x* axis and *y* axis [9].

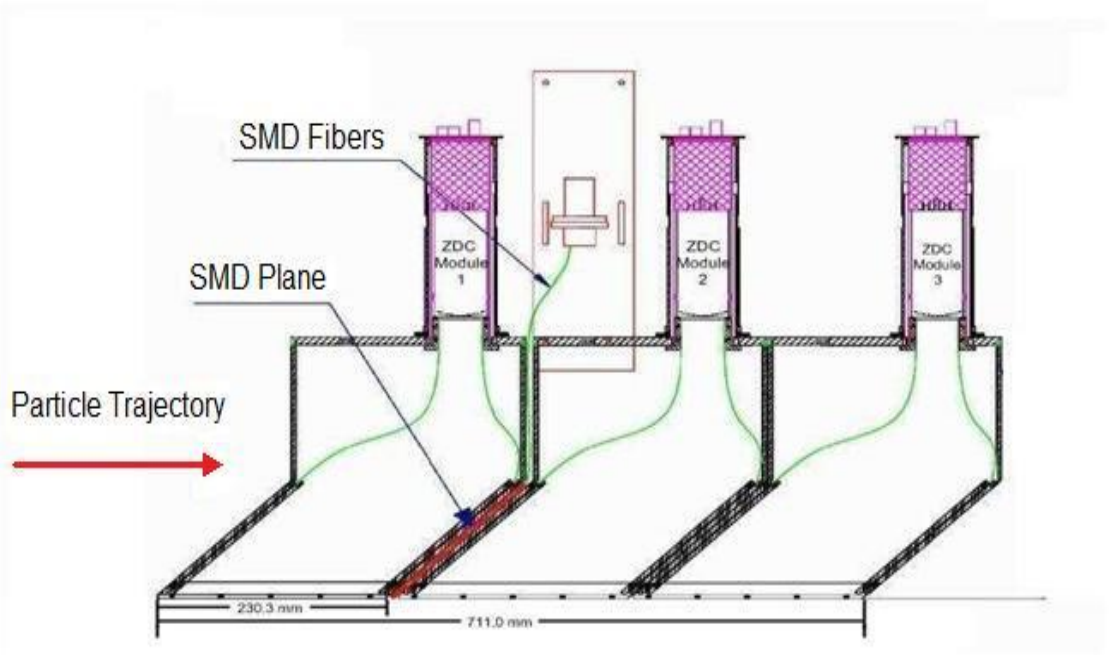

Fig. 4: Diagram of a Zero Degree Calorimeter. It consists of three identical calorimeter modules tilted at a 45 degree angle with respect to the beam. The Shower Max Detector (SMD) is located between ZDC module 1 and module 2 [6].

each strip is a fiber that collects light from the scintillator and then transports it to a 16-channel multi-anode photomultiplier tube (MAPMT). As shown in Fig. 6, the horizontal strips are positioned with their long axis horizontal as to provide vertical position information while the vertical strips provide horizontal positions.

The scintillator strips are grouped together to form slats; four strips comprise each horizontal slat and 3 strips each vertical slat. Each channel of the MAPMT measures the collected light from one slat and connects to an analog-to-digital converter (ADC) to provide pulse-height data. Shown in Fig.6, the slats are combined together to create a vertical (7 slats) and horizontal (8 slats) SMD plane. Each SMD plane's overall dimensions are approximately 16.5 cm in length x 11 cm wide x 1 cm thick. The

horizontal and vertical SMD planes are adjacent to each other, in a manner that a particle entering the SMD will have both vertical and horizontal positions measured.

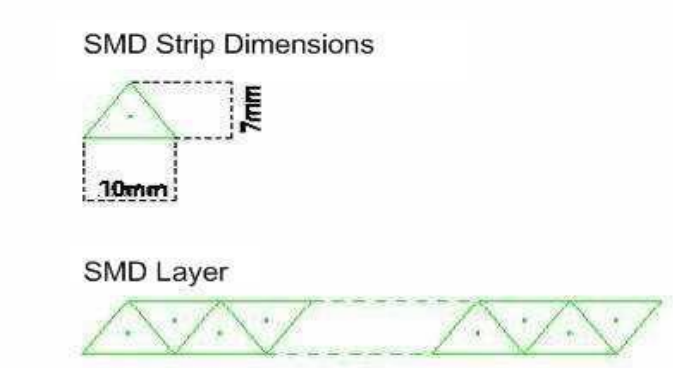

Fig. 5: Diagram of the SMD strips. Dimensions of an individual strip are included as well as positioning of strips to form a plane [6].

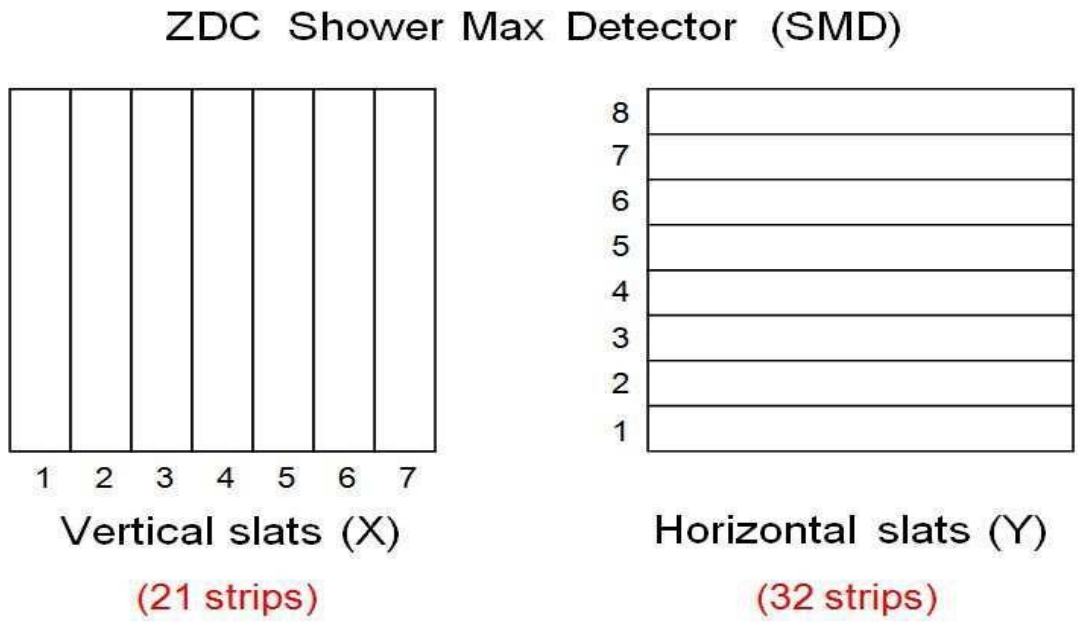

Fig. 6: Diagram of SMD planes. The positions of the slats are shown for both vertical and horizontal SMD planes [6].

Chapter III

Data Analysis

This analysis used thirty data-taking periods (runs) totaling approximately 27 million events of ZDC SMD data. The runs were spread over periods when protons are injected and then allowed to collide, called fills, three of which are between March 13-15, 2009, and one on March 22, 2009; refer to Appendix A for run numbers. All events are polarized proton-proton interactions with beam energies of 250 GeV for each polarized proton beam, which makes a center of mass energy ($\sqrt{s}$) of 500 GeV.

During fills using polarized-protons, each beam is injected into the RHIC storage ring with a specific spin pattern of beam protons polarized transversely-normal up, transversely-normal down, and unfilled bunches. Each circulating beam contains 120 bunches of protons, with each bunch being polarized as desired. The spin states for each bunch of both the blue and yellow beams for all fills used in the sample (found in Appendix B) have four possible interaction states: yellow up, blue up; yellow up, blue down; yellow down, blue up; and yellow down, blue down. Since a neutron production asymmetry [16] on both the east and west side of STAR is used in this analysis, only events with bunches where both beams are polarized were analyzed. The events with unfilled bunches were not analyzed. Both a "forward" and "backward" physics asymmetry is calculated. "Forward" refers to the direction that the beam, being used for calculation, is traveling after the interaction region, with "backward" referring to the opposite direction.

In order for the energy response of each ADC channel for each slat to be comparable to another, a correction must be made. A typical example of an ADC spectrum (counts vs. ADC channel) for one slat in the ZDC SMD for one run is shown in Fig. 7. Each ADC spectrum contains a nonzero minimum value called the pedestal, corresponding to a zero energy hit. This pedestal value is typical of an ADC and must be corrected to get the relative "energy." The energy correction is done by fitting a Gaussian peak to find the pedestal of each slat, then subtracting that peak's mean from a measured ADC value from an event. Figure 7 shows a typical fit of a pedestal for any given slat. Equation (1) is used to calculate the relative energy of each hit in each slat,

$$\text{Energy} = (\text{ADC value} - \text{pedestal}) * (\text{gain ratio}). \quad (1)$$

After the pedestal subtraction, the ADC value must be corrected so that each slat's calculated "energy" can be comparable to the "energy" of any other slat. Note that "energy" is not an absolute measurement. For the method of weighting being used, this correction is essential to ensuring uniformity of energy calculations in the detector. An exponential fit was applied between ADC values of 50 and 200, as shown in Fig. 8. This region was chosen because it is one of the most uniform portions of the ADC spectrum for all slats. Once the fit is done, the inverse of the slope parameter of the exponential function can be used as a gain ratio providing a multiplicative factor for the ADC value of the slat. Entering the pedestal and exponential slope parameter into equation (1) yields an energy of arbitrary units.

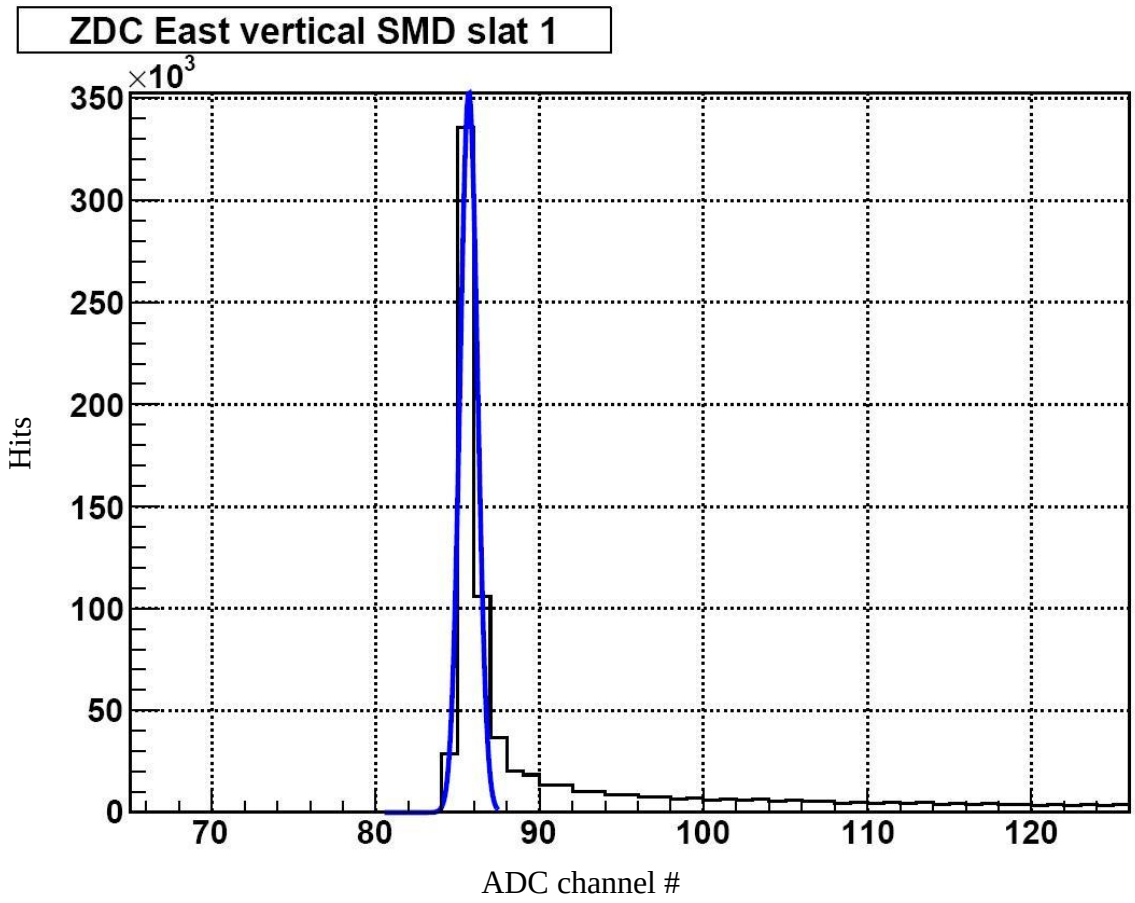

Fig. 7: Sample of a typical graph of counts versus ADC for a ZDC SMD slat. This graph depicts data from a typical run. A Gaussian fit of the pedestal is shown in blue.

To find an angular asymmetry for a rectangular detector, the detector needs to be split into angular (phi) bins about the center of the detector. Since the detector is at a 45 degree slant, the vertical axis of the SMD plane needs to be corrected. This correction is done by defining the phi bins on the projection of the SMD plane that is perpendicular to the beam lines; see Fig. 9. Defining the phi bins on the projection of the SMD plane reduces the effective area of the detector (11.7 cm tall x 11 cm wide). Figure 10 shows the phi bin definitions on the projection of the SMD's plane. Each phi bin covers an

angle of π/6 arranged in a way that both the *x* and *y* axes of the plane are in the middle of one of

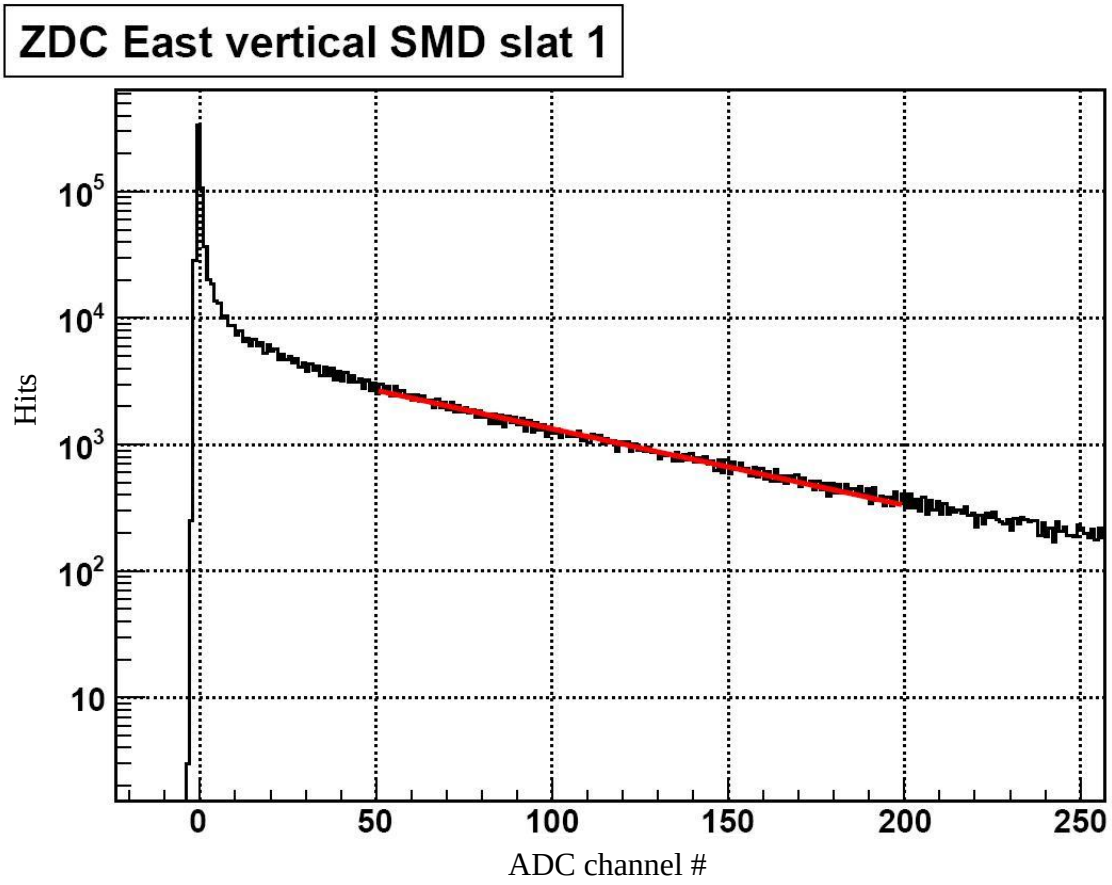

Fig. 8: Sample of a typical graph of pedestal subtracted counts versus ADC for a ZDC SMD slat. This graph depicts data from a typical run. An exponential fit of the gain is shown in red.

the phi bins. The phi bins are defined in this manner so that both the maxima ($\phi = 0$) and minima ($\phi = \pi/2$) of the left-right physics asymmetry can be measured. Each phi bin is not equal in surface area, but this is not required for this asymmetry analysis. The analysis only compares the hits in phi bin 1 to the hits in phi bin 7, phi bin 2 to phi bin 8,

and so on. Each phi bin and its complementary phi bin (e.g. phi bin 1 and phi bin 7) are equal in surface area.

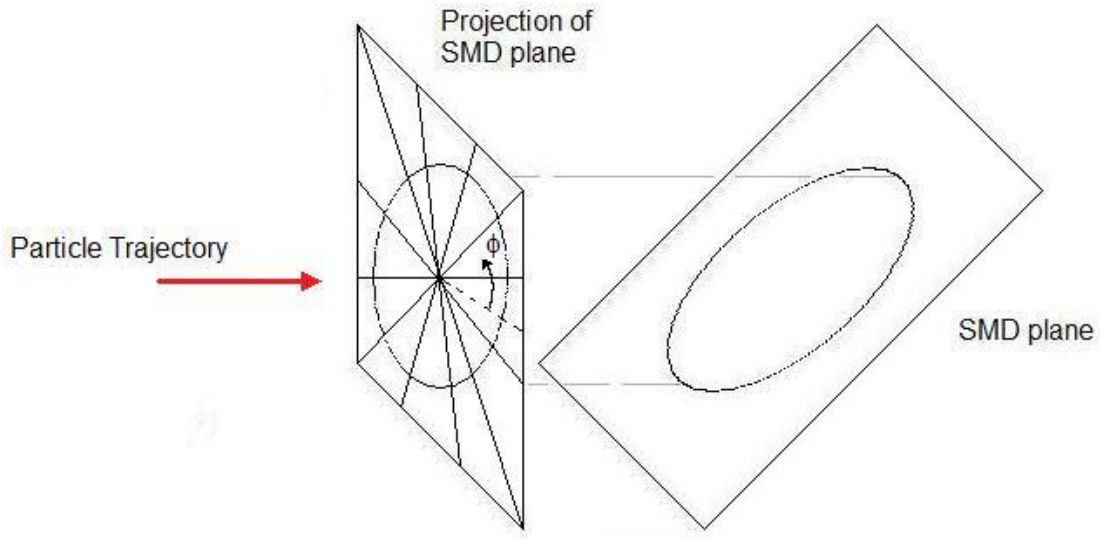

Fig. 9: Diagram showing the actual SMD plane tilted 45 degrees and the projection of the SMD plane.

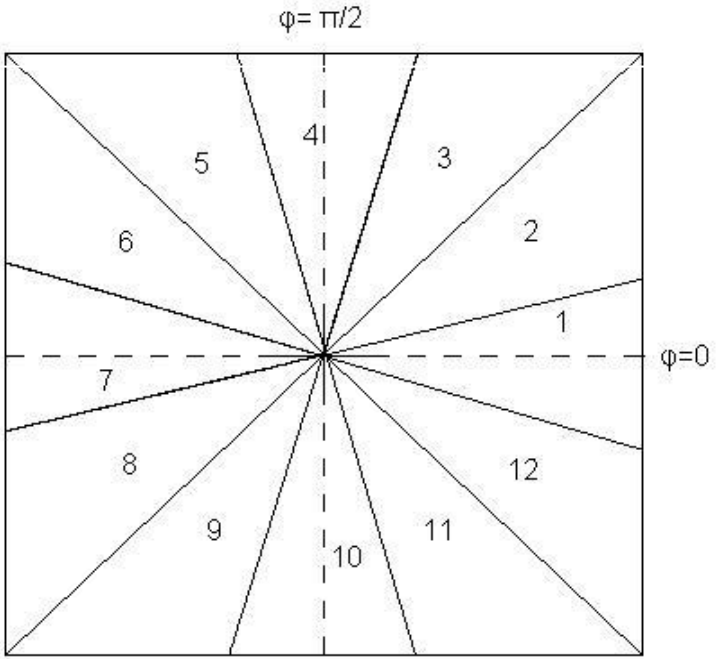

Fig. 10: Diagram showing phi bin definitions. Phi bin definitions are number 1-12 and are separated by solid lines. The dotted lines show the *x* and *y* axis on the plane of the SMD's projection.

The ZDC SMD data are further split into four categories, which are based upon the spin states of the beams. For each east and west ZDC detector, the data are split into whether or not the blue beam had its spin direction up or down and the yellow beam was up or down. The eight data categories, along with their requirements, are shown in Table 1. Since the yellow beam is traveling towards the east ZDC, the EYU (east yellow up) and EYD (east yellow down) categories will be used to calculate the single-spin, forward physics asymmetry for the yellow beam, while the west detector (WYU and WYD categories) will be used to calculate the single-spin, backward physics asymmetry for the yellow beam. Likewise, the west detector (WBU and WBD categories) will be used to calculate the single-spin, forward physics asymmetry for the blue beam, and the east detector (EBU and EBD categories) will be used to calculate the single-spin, backwards asymmetry for the blue beam.

Data Categories				
Category	Abbreviation	ZDC	Yellow Polarization	Blue Polarization
East, yellow up	EYU	East	+	+ or -
East, yellow down	EYD	East	-	+ or -
East, blue up	EBU	East	+ or -	+
East, blue down	EBD	East	+ or -	-
West, yellow up	WYU	West	+	+ or -
West, yellow down	WYD	West	-	+ or -
West, blue up	WBU	West	+ or -	+
West, blue down	WBD	West	+ or -	-

Table 1: Data categories of detector, beams, and spin-state combinations. Each row includes the category, abbreviation used in the text, detector, and the possible spin states of the beams that would provide a hit in that category.

This single-spin asymmetry analysis requires that only one beam polarization is kept in the same state (up or down) for each category; the spin states of the second beam are averaged over both up and down states. The "hits" in an SMD detector attributed to each one of these eight categories are then analyzed to find the position of each hit using an energy-centroid method.

The energy-centroid method calculates the *x* (horizontal) and *y* (vertical) energy-weighted position using the equations below:

$$x_{\text{hit}} = \frac{\sum_1^7 x_{\text{vert slat i}} * E_{\text{vert slat i}}}{\sum_1^7 E_{\text{vert slat i}}} \quad \text{and} \quad y_{\text{hit}} = \frac{\sum_1^8 y_{\text{hori slat i}} * E_{\text{hori slat i}}}{\sum_1^8 E_{\text{hori slat i}}} \; . \qquad (2)$$

Figure 11 shows the *x* and *y* positions for both the east and west detectors for 10 000 events from a typical run. A minimum total "energy" requirement is placed on each SMD plane and events that fail have positions assigned with zero position for that plane. Note that these events assigned positions (0,0) will be dropped from the data sample later, since no angle can be calculated from a zero radius.

Due to the energy-weighting method, a binning effect was observed when only one slat for each of the vertical and horizontal slats is hit. This effect creates a high density in the middle of the slat, as observed in Fig. 11. An energy threshold was implemented to correct the binning effect. Energy deposited in each slat was summed to determine the total energy per plane and also for the event. The total energy threshold was chosen so that the energy from a hit in a single slat would never exceed that value. After the energy-weighted *x* and *y* positions were found for each hit, the angle φ and the

radius can be calculated with simple trigonometry. Each hit is then placed into its corresponding phi bin. A minimum radius threshold of 0.5 cm was implemented to reduce the possibility of hits being counted in the wrong phi bin due to the energy weighting.

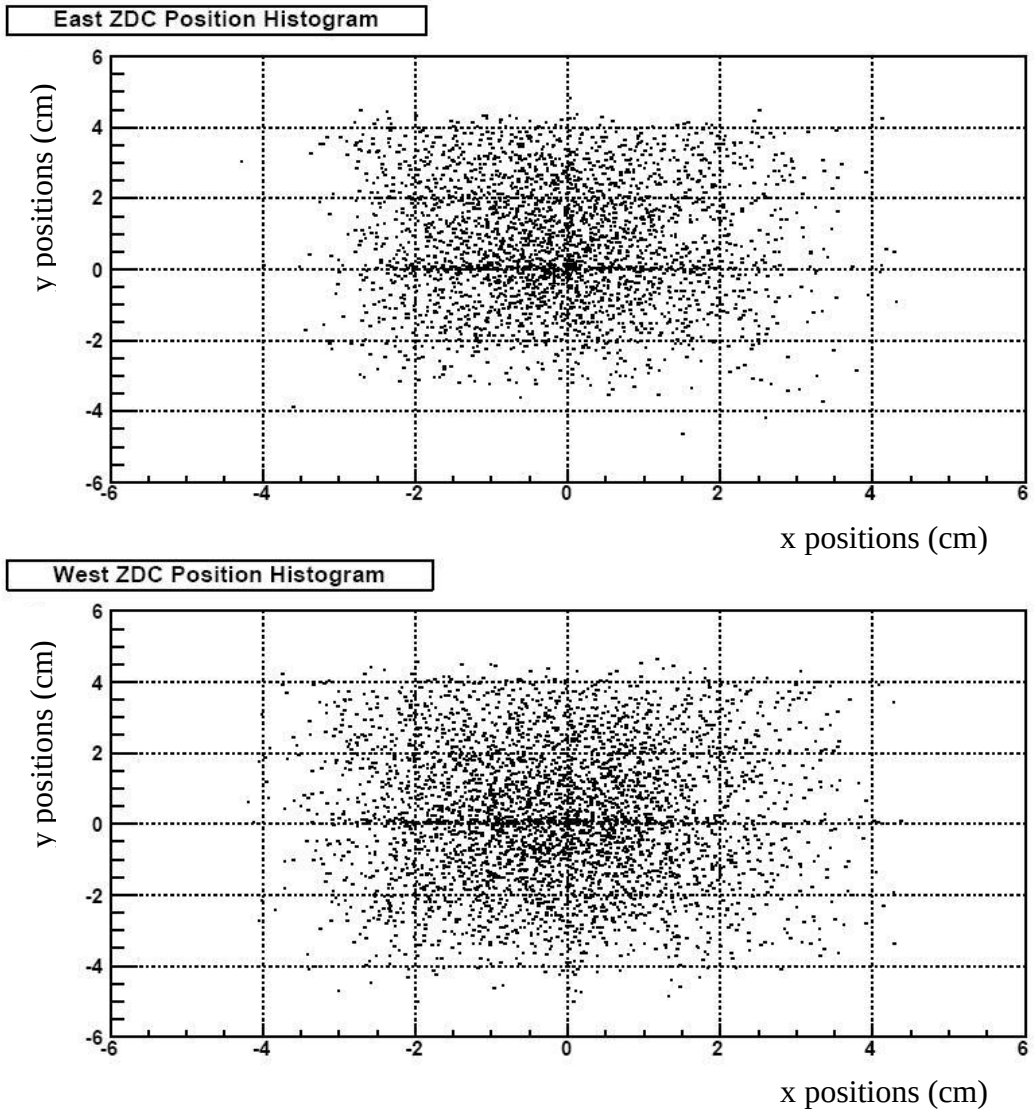

Fig. 11: Histograms showing the energy-weighted *x* and *y* positions of both the east and west detectors for 10 000 events.

The phi bin definitions discussed above are then applied to each category of data. The number of hits in each phi bin is then entered into a histogram for each of the eight spin state/detector categories. Figure 12 shows a sample histogram with all cuts for phi bin 1. Figure 13 shows a histogram of hits per phi bin for the four forward categories. As indicated in Fig. 13, the WBU and WBD histograms have roughly the same number of hits and have the same basic shape, which shows that the beam has approximately the same distribution over the detector for both spin states, up and down. This is also true for EYU and EYD, as shown in Fig. 13. The same pattern was observed for WYU and WYD, and also for EBU and EBD. This similar pattern within each pair, such as EYU and EYD, is an early indication that the calculated physics asymmetry will be small. Differences between each pair, for example, WBU/WBD compared to EYU/EYD, may be due to detector or beam differences.

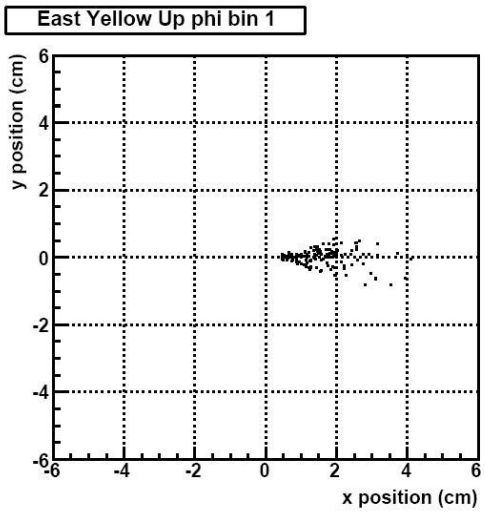

Fig. 12: Data sample of hits in phi bin 1. All data cuts are included for this histogram.

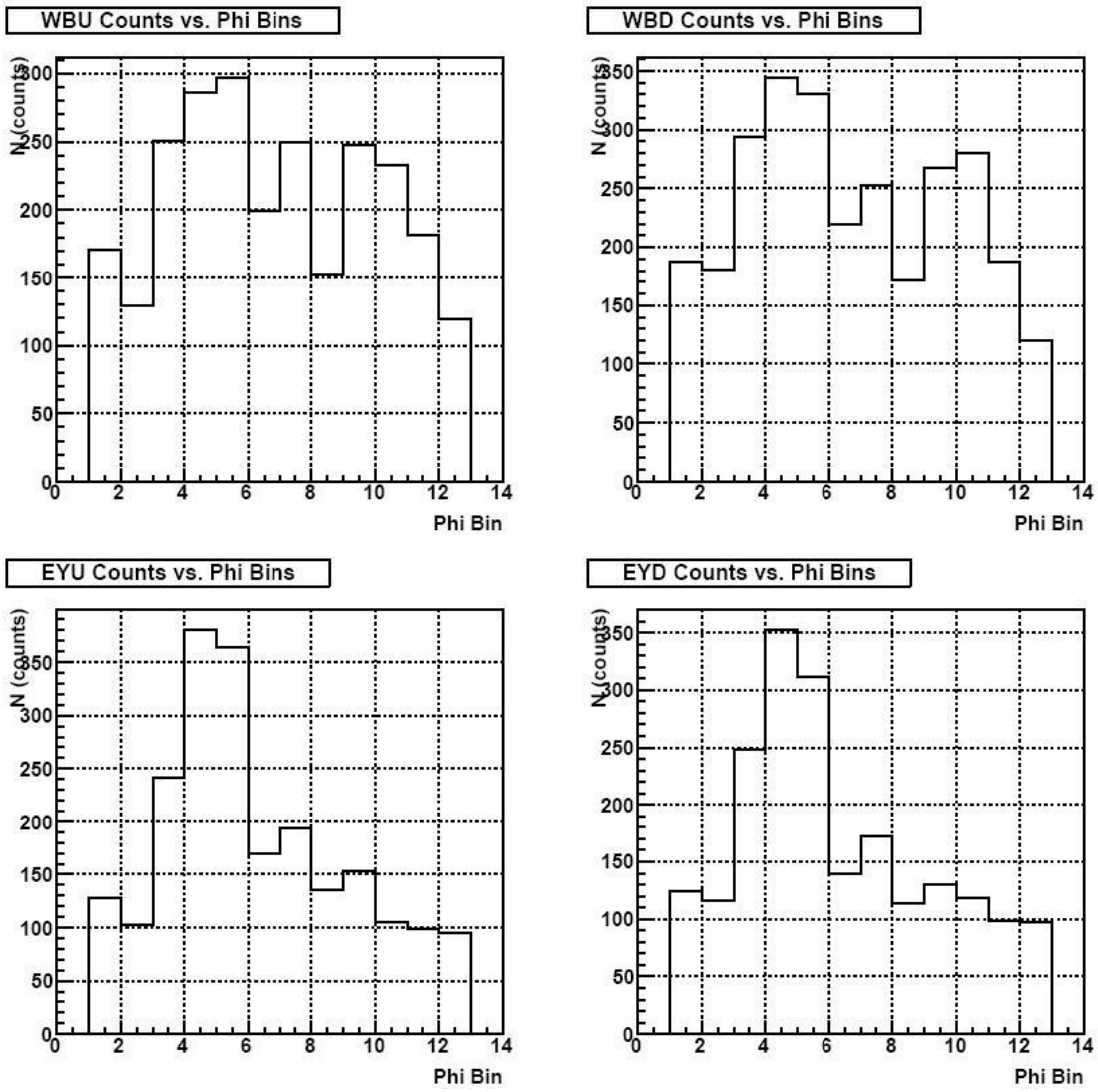

Fig. 13: Frequency of hits per phi bin for the forward categories. Data are from a typical run. Each histogram represents a data category described in Table 1.

The polarimeters of the RHIC ring are used to measure the overall absolute polarization in the stable (transversely-normal) spin state of both the blue and yellow beams. Two types of polarimeters [17] are used together to measure the absolute polarization of the beams. The first type uses a carbon fiber that is inserted into the beam

line and measures a left-right asymmetry of recoiling carbon nuclei. The second type involves a polarized hydrogen jet located within the beam to measure a left-right asymmetry of elastic proton-proton scattering. Both polarimeters utilize the interference between electromagnetic and nuclear forces, called Coulomb-nuclear interference (CNI) [18]. At RHIC, the hydrogen-jet polarimeter provides the absolute polarization, while the carbon-fiber polarimeter provides measurements that give relative polarizations to the hydrogen-jet polarization [8]. These two methods used together provide the absolute polarization of the beams during a fill (approx. 2 hours). Table 2 shows the absolute polarizations of each beam for each sample fill used.

Absolute Beam Polarization			
Fill	Yellow Polarization	Blue Polarization	Polarization
10364	0.4596 ± 0.0887	0.3376 ± 0.0654	transversely normal
10372	0.0000 ± 0.0000	0.0000 ± 0.0000	unpolarized
10373	0.4678 ± 0.0902	0.4800 ± 0.0925	transversely normal
10407	0.3141 ± 0.0607	0.2392 ± 0.0463	longitudinal

Table 2: Time-averaged absolute polarizations of both yellow and blue beams for each fill. These values are taken from analyses of the data from the CNI polarimeters. Note that in fill 10372 the beam was not polarized, in fill 10407 the beam is longitudinally polarized, and in fill 10364 and 10373 the beam is transversely polarized [19-21].

The asymmetry for each phi bin and its complementary phi bin (e.g. phi bin 1 and phi bin 7) are calculated using the square-root-asymmetry equation,

$$\epsilon_{phys} = \frac{\sqrt{N_L^{\uparrow} N_R^{\downarrow}} - \sqrt{N_L^{\downarrow} N_R^{\uparrow}}}{\sqrt{N_L^{\uparrow} N_R^{\downarrow}} + \sqrt{N_L^{\downarrow} N_R^{\uparrow}}}. \quad (3)$$

The number of hits calculated from a given phi bin corresponds to N. The up arrow (↑) represents the number of hits in a phi bin when the specified beam is polarized transversely up, and the down arrow (↓) for those hits when the beam is polarized transversely down. The quantities L and R refer to that portion of the detector on which the particle hit occurred. In the analysis, the R portion of the detector consists of phi bins 1-6 while the L portion consists of phi bins 7-12. Note that these detector designations are not physically the left and right side of the detector. This is done for all four combinations of detector (east and west) and beam (yellow and blue), with each combination corresponding to the forward or backward asymmetry for the beam. Table 3 shows the four combinations of detector and beam and the calculated asymmetry names.

The asymmetry calculated from each pair of phi bins in given by the equation,

$$\epsilon(\varphi) = \epsilon_N \cos(\varphi) + \epsilon_S \sin(\varphi). \qquad (4)$$

In the fit, the parameter ϵ_N refers to the transverse-normal asymmetry. This is given by parameter "p1" in Figure 14, and ϵ_S refers to the sideways asymmetry parameter "p2" in Figure 14. The parameter "p0" in Figure 14 refers to an asymmetry offset constant. The figure also displays the calculated phi asymmetry $\epsilon(\varphi)$ for each pair of phi bins, as well as a fit of the data, using equation (4). The transverse and sideways asymmetries for all fills are shown in Table 4.

The analyzing power (A_N) and the calculated asymmetry (ϵ_N) are based on the physics of the spin interaction causing the asymmetry. The equation below relates the analyzing power and the single-spin, transversely-normal physics asymmetry, with *P*

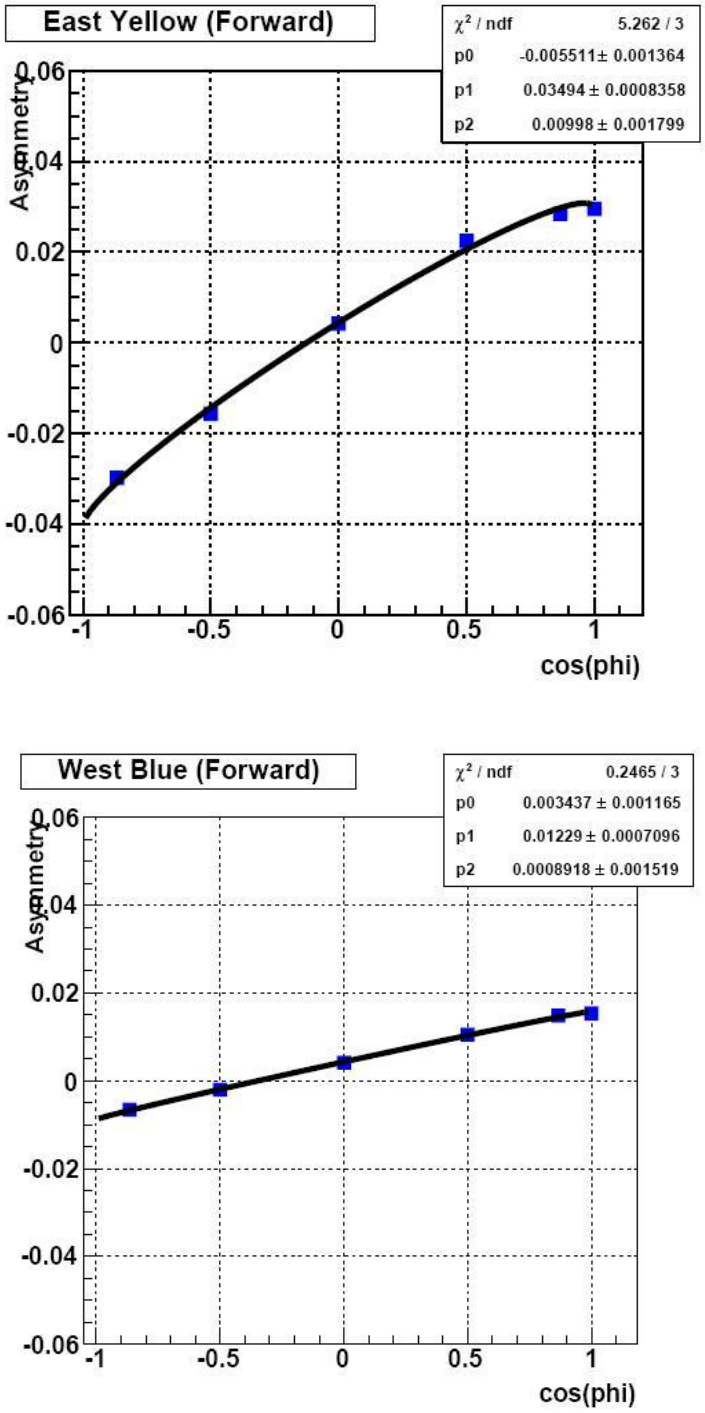

Fig. 14: Graphs of asymmetry vs. cos(φ) for both east and west detector forward asymmetries. The displayed parameter p1 corresponds to ϵ_N and parameter p2 corresponds to ϵ_S

Asymmetry for Detector/Beam Combination		
Detector	Beam	Asymmetry
East ZDC	Yellow beam	Forward yellow asymmetry
East ZDC	Blue beam	Backward yellow asymmetry
West ZDC	Yellow beam	Backward blue asymmetry
West ZDC	Blue beam	Forward blue asymmetry

Table 3: Each detector/beam combination and the asymmetries that result from the square-root-asymmetry equation (Eq. 1).

Beam - Detector Combination					
Fill	Asymmetry	Forward Yellow	Backward Yellow	Forward Blue	Backward Blue
10364	ε (normal)	0.0350 ± 0.0008	0.0034 ± 0.0007	0.0123 ± 0.0007	0.0020 ± 0.0008
	ε (sideways)	0.0100 ± 0.0018	-0.0008 ± 0.0015	0.0009 ± 0.0015	-0.0019 ± 0.0018
10372	ε (normal)	-0.0019 ± 0.0012	0.0013 ± 0.0011	-0.0020 ± 0.0011	-0.0023 ± 0.0012
	ε (sideways)	0.0010 ± 0.0027	0.0006 ± 0.0024	0.0000 ± 0.0024	-0.0032 ± 0.0027
10373	ε (normal)	0.0384 ± 0.0009	0.0020 ± 0.0008	0.0173 ± 0.0008	-0.0006 ± 0.0009
	ε (sideways)	0.0108 ± 0.0019	0.0022 ± 0.0016	0.0056 ± 0.0016	0.0024 ± 0.0019
10407	ε (normal)	0.0011 ± 0.0005	0.0001 ± 0.0005	0.0009 ± 0.0005	0.0001 ± 0.0005
	ε (sideways)	0.0002 ± 0.0011	0.0018 ± 0.0010	-0.0034 ± 0.0010	-0.0015 ± 0.0011

Table 4: Calculated single-spin physics transversely-normal and sideways asymmetries for the forward and backward directions of each beam.

being the polarization of the beam,

$$A_N = \frac{\epsilon_N}{P}. \tag{5}$$

The proof of this equation is given in Appendix C. From equation (5), A_N is calculated for both the yellow and blue beams using the transverse asymmetry, ϵ_N, using approximately 6 million events. The analyzing power for center-of-mass energy of 500

GeV, for the yellow beam was found to be A_N = 0.0762 ± 0.0148, and the analyzing power for the blue beam was found to be A_N = 0.0364 ± 0.0074. The difference in analyzing powers between the two beams may be due to a difference in background hits in the detectors. Note the dominant source of error for the analyzing powers is due to error in the absolute polarization measurements. The analyzing powers can then be used to calculate beam polarizations for any transversely-normal or sideways asymmetry using this method for these detectors.

Chapter IV

Results and Conclusions

The beam polarization calculations use the same equation given above, but are rearranged to find the polarization,

$$P_N = \frac{\epsilon_N}{A_N} \qquad \text{and} \qquad P_S = \frac{\epsilon_S}{A_S}. \qquad (6)$$

By inserting the analyzing power values calculated above, along with the transversely-normal asymmetry (ϵ_N) and sideways asymmetry (ϵ_S) of each fill for both beams into equation (6), both the transverse-normal polarization component (P_N) and sideways polarization component (P_S) of the local polarization can be found. The transverse analyzing power, A_N, is equal to the sideways analyzing power ($A_S = A_N$) since it is the same interaction, but now rotated 90 degrees. Table 5 shows the transverse and sideways polarization components for fills 10372, 10373, and 10407.

ZDC SMD Polarization				
Fill	Yellow Transverse Polarization	Yellow Sideways Polarization	Blue Transverse Polarization	Blue Sideways Polarization
10372	-0.0025 ± 0.0164	0.0132 ± 0.0354	-0.0561 ± 0.0330	0.0000 ± 0.0317
10373	0.5035 ± 0.0985	0.1417 ± 0.0373	0.4745 ± 0.0987	0.0734 ± 0.0256
10407	0.0151 ± 0.0074	0.0021 ± 0.0147	0.0257 ± 0.0139	-0.0442 ± 0.0158

Table 5: The calculated, transversely-normal and sideways polarization components for both beams during 3 sample fills. Fill 10372 was unpolarized, fill 10373 was polarized transversely-normal, and fill 10407 was longitudinally polarized.

The local polarizations can then be found from the analyzing powers using equation (6). The local transverse polarizations using a different set of sample data yields a transverse polarization of P_N = 0.5035 ± 0.0985 for the yellow beam and a transverse polarization of P_N = 0.4745 ± 0.0985 for the blue beam. These values are consistent within statistics with the absolute transverse polarization measurements from the CNI detectors of P_N = 0.4678 ± 0.0902 for the yellow beam [20] and P_N = 0.4800 ± 0.0925 for the blue beam [21] over the same fill. This analysis also provides a sideways polarization of P_S = 0.1417 ± 0.0373 for the yellow beam and a sideways polarization of P_S = 0.0734 ± 0.0256 for the blue beam. Knowing the sideways components of the beams locally at STAR provides important corrections to calculations involving beam polarization in spin measurements.

As displayed in Table 5, the transverse and sideways components of both the unpolarized fill (fill 10372) and the longitudinally-polarized fill (fill 10407) are consistent with zero, as expected. The exception is a nonzero value for the blue beam sideways component of P_S = -0.0442 ± 0.0158 for fill 10407. This nonzero sideways component could mean that the blue beam contained a small sideways component while in the RHIC storage ring, or that the spin rotators for the blue beam were placing a small sideways component during rotation from normal spin state to longitudinal spin state. All backwards asymmetries are either consistent with zero or very small. This is an expected result because each detector's incoming beam, yellow for east and blue for west, was averaged over both spin states for the other beam (e.g. polarization is approximately zero).

If the values were nonzero, this would indicate that the polarization of the beam was not averaging to zero.

Knowing the analyzing power of the spin interactions at the ZDC (very far forward) for proton-proton collisions at $\sqrt{s}$ =500 GeV will allow STAR to be able to measure the local polarization at the intersection region. This measurement means that the absolute polarization of both beams, including transverse and sideways components, can be found locally at STAR. The result of this measurement can also allow more accurate calculations to be performed for spin-spin interaction analyses. The ability to measure transverse and sideways components may then be used to check the functionality of the spin rotators during longitudinally-polarized beams.

In further analyses of ZDC data, it may be useful to implement a coincidence requirement between the ZDC SMDs, other STAR detectors, and the ZDCs (calorimeters, not SMDs). This requirement will ensure that sufficient energy is deposited into the calorimeters in order for position calculations to be made, and will reduce any background hits found in the ZDC SMDs.

Another useful analysis would be to investigate the large difference in analyzing powers between the east and west ZDCs. It is expected that both would have the roughly the same analyzing power, since they are constructed in the same manner and placed in the same locations on either side of the STAR interaction region.

Appendix A

Table 6 below shows the run numbers for each fill that were used for the sample data of the analysis. Each run contains approximately one million events.

Sample Data	
Fill #	Run #
10364	10072078, 10072096, 10072097, 10072106, 10072107, 10072112
10372	10074051, 10074052, 10074053, 10074054, 10074055, 10074056
10373	10074062, 10074064, 10074065, 10074069, 10075011, 10075012
10407	10081003, 10081016, 10081018, 10081020, 10081025, 10081030, 10081043, 10081045, 10081048, 10081057, 10081058, 10081059

Table 6: Fill numbers (first column) and the run numbers corresponding to each fill (second column).

Appendix B

Figures 15-18 show the bunch crossing spin states for each bunch of protons for all sample fills used in this analysis. In Figure 15-17 a (+) sign indicates a beam spin transversely polarized up while a (–) indicates spin transversely down. In Figure 18 a (+) sign indicates a beam spin longitudinally polarized forward (positive helicity) while a (–) indicates spin longitudinally polarized backward (negative helicity). Unfilled or unused bunches are represented by a 0. The large section of unfilled bunches at the end of row one and row two of each table represents the abort gap, an empty section of each beam used when removing the beams from the RHIC storage rings.

Fill No.																																					
10364										1										2									3									4
Bunch	1	2	3	4	5	6	7	8	9	0	1	2	3	4	5	6	7	8	9	0	1	2	3	4	5	6	7	8	9	0	1	2	3	4	5	6	7	8	9	0
Yellow	+	+	-	-	+	+	-	-	+	+	-	-	+	+	-	-	+	+	-	-	+	+	-	-	+	+	-	-	+	+	-	0	0	0	0	0	0	0	0	0
Blue	+	-	+	-	-	+	-	+	+	-	+	-	-	+	-	+	+	-	+	-	-	+	-	+	+	-	+	-	-	+	-	0	0	0	0	0	0	0	0	0
	4									5										6									7									8
Bunch	1	2	3	4	5	6	7	8	9	0	1	2	3	4	5	6	7	8	9	0	1	2	3	4	5	6	7	8	9	0	1	2	3	4	5	6	7	8	9	0
Yellow	+	+	-	-	+	+	-	-	+	+	-	-	+	+	-	-	+	+	-	-	+	+	-	-	+	+	-	-	+	+	-	-	+	+	-	-	+	+	-	-
Blue	+	-	+	-	-	+	-	+	+	-	+	-	-	+	-	+	+	-	+	-	-	+	-	+	+	-	+	-	-	+	-	+	+	-	+	-	-	+	-	+
																				1									1									1
	8									9										0									1									2
Bunch	1	2	3	4	5	6	7	8	9	0	1	2	3	4	5	6	7	8	9	0	1	2	3	4	5	6	7	8	9	0	1	2	3	4	5	6	7	8	9	0
Yellow	+	+	-	-	+	+	-	-	+	+	-	-	+	+	-	-	+	+	-	-	+	+	-	-	+	+	-	-	+	+	-	0	0	0	0	0	0	0	0	0
Blue	+	-	+	-	-	+	-	+	+	-	+	-	-	+	-	+	+	-	+	-	-	+	-	+	+	-	+	-	-	+	-	0	0	0	0	0	0	0	0	0

Table 7: Spin states for each bunch of both the blue and yellow beams for fill 10364.

Fill No.																																						
10372										1										2									3									4
Bunch	1	2	3	4	5	6	7	8	9	0	1	2	3	4	5	6	7	8	9	0	1	2	3	4	5	6	7	8	9	0	1	2	3	4	5	6	7	8	9	0
Yellow	-	-	+	0	+	-	-	0	+	+	-	0	-	+	+	0	-	-	+	0	+	-	-	0	+	+	-	0	-	+	+	0	0	0	0	0	0	0	0	0
Blue	+	-	+	0	-	-	+	0	-	+	+	0	-	+	-	0	-	+	-	0	+	+	-	0	+	-	-	0	+	-	+	0	0	0	0	0	0	0	0	0
	4									5										6									7									8
Bunch	1	2	3	4	5	6	7	8	9	0	1	2	3	4	5	6	7	8	9	0	1	2	3	4	5	6	7	8	9	0	1	2	3	4	5	6	7	8	9	0
Yellow	-	-	+	0	+	-	-	0	+	+	-	0	-	+	+	0	-	-	+	0	+	-	-	0	+	+	-	0	-	+	+	0	-	-	+	0	+	-	0	0
Blue	-	+	+	0	-	+	-	0	-	+	-	0	+	+	-	0	+	-	-	0	+	-	+	0	+	-	+	0	-	-	+	0	-	+	+	0	-	+	0	0
																				1									1									1
	8									9										0									1									2
Bunch	1	2	3	4	5	6	7	8	9	0	1	2	3	4	5	6	7	8	9	0	1	2	3	4	5	6	7	8	9	0	1	2	3	4	5	6	7	8	9	0
Yellow	+	+	-	0	-	+	+	0	-	-	+	0	+	-	-	0	+	+	-	0	-	+	+	0	-	+	+	0	-	+	-	0	0	0	0	0	0	0	0	0
Blue	-	+	-	0	+	+	-	0	+	-	-	0	+	-	+	0	+	-	+	0	-	-	+	0	-	+	+	0	-	+	-	0	0	0	0	0	0	0	0	0

Table 8: Spin states for each bunch of both the blue and yellow beams for fill 10372.

Fill No.																																						
10373										1										2									3									4
Bunch	1	2	3	4	5	6	7	8	9	0	1	2	3	4	5	6	7	8	9	0	1	2	3	4	5	6	7	8	9	0	1	2	3	4	5	6	7	8	9	0
Yellow	-	-	+	0	+	-	-	0	+	+	-	0	-	+	+	0	-	-	+	0	+	-	-	0	+	+	-	0	-	+	+	0	0	0	0	0	0	0	0	0
Blue	+	-	+	0	-	-	+	0	-	+	+	0	-	+	-	0	-	+	-	0	+	+	-	0	+	-	-	0	+	-	+	0	0	0	0	0	0	0	0	0
	4									5										6									7									8
Bunch	1	2	3	4	5	6	7	8	9	0	1	2	3	4	5	6	7	8	9	0	1	2	3	4	5	6	7	8	9	0	1	2	3	4	5	6	7	8	9	0
Yellow	-	-	+	0	+	-	-	0	+	+	-	0	-	+	+	0	-	-	+	0	+	-	-	0	+	+	-	0	-	+	+	0	-	-	+	0	+	-	0	0
Blue	-	+	+	0	-	+	-	0	-	+	-	0	+	+	-	0	+	-	-	0	+	-	+	0	+	-	+	0	-	-	+	0	-	+	+	0	-	+	0	0
																				1									1									1
	8									9										0									1									2
Bunch	1	2	3	4	5	6	7	8	9	0	1	2	3	4	5	6	7	8	9	0	1	2	3	4	5	6	7	8	9	0	1	2	3	4	5	6	7	8	9	0
Yellow	+	+	-	0	-	+	+	0	-	-	+	0	+	-	-	0	+	+	-	0	-	+	+	0	-	-	+	0	+	-	-	0	0	0	0	0	0	0	0	0
Blue	-	+	-	0	+	+	-	0	+	-	-	0	+	-	+	0	+	-	+	0	-	-	+	0	-	+	+	0	-	+	-	0	0	0	0	0	0	0	0	0

Table 9: Spin states for each bunch of both the blue and yellow beams for fill 10373.

Fill No.																																					
10407										1									2									3									4
Bunch	1	2	3	4	5	6	7	8	9	0	1	2	3	4	5	6	7	8	9	0	1	2	3	4	5	6	7	8	9	0	1	2	3	4	5	6	7	8	9	0
Yellow	-	-	+	+	-	-	+	+	-	-	+	+	-	-	+	+	-	-	+	+	-	-	+	+	-	-	+	+	-	-	+	0	0	0	0	0	0	0	0	0
Blue	+	-	+	-	-	+	-	+	+	-	+	-	-	+	-	+	+	-	+	-	-	+	-	+	+	-	+	-	-	+	-	0	0	0	0	0	0	0	0	0
	4									5									6									7									8
Bunch	1	2	3	4	5	6	7	8	9	0	1	2	3	4	5	6	7	8	9	0	1	2	3	4	5	6	7	8	9	0	1	2	3	4	5	6	7	8	9	0
Yellow	-	-	+	+	-	-	+	+	-	-	+	+	-	-	+	+	-	-	+	+	-	-	+	+	-	-	+	+	-	-	+	+	-	-	+	+	-	-	+	+
Blue	+	-	+	-	-	+	-	+	+	-	+	-	-	+	-	+	+	-	+	-	-	+	-	+	+	-	+	-	-	+	-	+	+	-	+	-	-	+	-	+
																			1									1									1
	8									9									0									1									2
Bunch	1	2	3	4	5	6	7	8	9	0	1	2	3	4	5	6	7	8	9	0	1	2	3	4	5	6	7	8	9	0	1	2	3	4	5	6	7	8	9	0
Yellow	-	-	+	+	-	-	+	+	-	-	+	+	-	-	+	+	-	-	+	+	-	-	+	+	-	-	+	+	-	-	+	0	0	0	0	0	0	0	0	0
Blue	+	-	+	-	-	+	-	+	+	-	+	-	-	+	-	+	+	-	+	-	-	+	-	+	+	-	+	-	-	+	-	0	0	0	0	0	0	0	0	0

Table 10: Spin states for each bunch of both the blue and yellow beams for fill 10407.

Appendix C

The four equations below describe the number of hits for an ideal detector. These equations assume the double-spin and parity-violating analyzing powers to be zero. For this example the yellow beam was chosen.

$$\begin{aligned} N_{\boldsymbol{L}}^{\uparrow} &= N_{\mathbf{0}} L^{\uparrow} d\Omega_L (1 + P_Y A_f - P_B A_b) \\ N_{\boldsymbol{L}}^{\downarrow} &= N_{\mathbf{0}} L^{\downarrow} d\Omega_L (1 - P_Y A_f + P_B A_b) \\ N_{\boldsymbol{R}}^{\uparrow} &= N_{\mathbf{0}} L^{\uparrow} d\Omega_R (1 - P_Y A_f + P_B A_b) \\ N_{\boldsymbol{R}}^{\downarrow} &= N_{\mathbf{0}} L^{\downarrow} d\Omega_R (1 + P_Y A_f - P_B A_b) \end{aligned} \tag{7}$$

The number of hits for the left region and right region of the detector are represented by N_L and N_R, respectively, with the ($\uparrow$) and ($\downarrow$) corresponding to the chosen beam's spin state for that event. The quantity N_0 is a normalization factor, while $L^{\uparrow}$ and $L^{\downarrow}$ are the beam luminosities of each state for the chosen beam. The solid angle of the detector is represented by $d\Omega_L$ and $d\Omega_R$, with the letters L and R again representing the region of the detector. Each beam's polarization is given by P_Y for the yellow beam and P_B for the blue beam. Lastly, A_f and A_b are the forward and backward analyzing power for the chosen beam.

These equations are substituted into the square-root-asymmetry equation below (eqn 3),

$$\epsilon_{phys} = \frac{\sqrt{N_L^{\uparrow} N_R^{\downarrow}} - \sqrt{N_L^{\downarrow} N_R^{\uparrow}}}{\sqrt{N_L^{\uparrow} N_R^{\downarrow}} + \sqrt{N_L^{\downarrow} N_R^{\uparrow}}}. \tag{3}$$

Assuming that the backwards analyzing power is zero and using the yellow beam as an example, eqn. (3) becomes,

$$\epsilon_{phys} = \frac{\left(N_0\sqrt{L^{\uparrow}L^{\downarrow}d\Omega_L d\Omega_R}\right)2P_Y A_f}{2\left(N_0\sqrt{L^{\uparrow}L^{\downarrow}d\Omega_L d\Omega_R}\right)}.$$

Conveniently, the normalization constant, luminosities, and solid angles all cancel from the asymmetry equation, leaving only the quantities of the physics asymmetry, the polarization of the incoming beam, and the forward analyzing power,

$$\epsilon_{phys} = P_Y A_f.$$

Similar calculations are done for the blue beam, with the polarizations P_Y and P_B swapping places in eqn. (7).

Acknowledgments

I would like to thank Dr. David Grosnick for his help as advisor for this analysis. I would also like to thank Drs. Alice Bridgeman, Hal Spinka, and Jason Webb, and Nathan Kellams for all the information and help they provided. Thanks to Valparaiso University for providing a summer assistantship supported by the United States Department of Energy, Office of Science, Division of Nuclear Physics under Contract No. DE-AC02-06CH11357 and Grant No. DE-FG02-88ER40416

References

[1] L. C. Bland, RIKEN Rev. **28**, 8 (2000)

[2] N. Saito, Nucl. Phys. A **368**, 375 (1998)

[3] A. Airapetian *et al.*, Phys. Rev. Let. **84**, 2584 (2000)

[4] K.H. Ackermann *et al.*, Nucl. Instrum. Meth. A**499**, 624 (2003).

[5] C. H. Whitten, in AIP Conference Proceedings 980, UCLA, Los Angeles, California, 2007 (unpublished).

[6] M.B. Bitters *et al.*, STAR note SN-0480, 2009 (unpublished).

[7] I. Alekseev *et al.*, Nucl. Instrum. Meth. A**499**, 392 (2003).

[8] I. Nakagawa *et al.*, in AIP Conference Proceedings 915, RIKEN, Wako, Saitama, Japan, 2007 (unpublished).

[9] C. Adler *et al.*, Nucl. Instrum. Meth. A**470**, 488 (2001).

[10] E. D. Courant, Annu. Rev. Nucl. Part. Sci. **53**, 1 (2003).

[11] Ya. S. Derbenev and A. M. Kondratenko, *Tenth International Conference on High Energy Accelerators*, Protvino, 1977 (IHEP, Protvino, 1977), Vol. II, p. 70; in *High Energy Physics with Polarized Beams and Polarized Targets*, Argonne, 1978, edited by G. H. Thomas, AIP Conf. Proc. No. 51 (AIP, New York, 1979), p. 292; Ya. S. Derbenev *et al.*, Part. Accel. **8**, 115 (1978).

[12] H. Spinka *et al.*, Czechoslovak Journal of Physics, Vol. 53, A22 (2003).

[13] M. Okamura *et al.*, Nucl. Instrum. Meth. A**452**, 53 (2000).

[14] W. W. MacKay *et al.*, in Particle Accelerator Conference Proceedings, Brookhaven National Laboratory, Upton, NY, 2003 (unpublished).

[15] Y. Fukao *et al.*, Phys. Lett. B**650**, 325 (2007).

[16] M. Togawa, Ph. D. thesis, Kyoto University, 2003.

[17] Y. Makdisi, in AIP Conference Proceedings 415, Brookhaven National Laboratory, RHIC Project, Upton, NY, 1998 (unpublished).

[18] B. Z. Kopeliovich and L. I. Lapidus, Yad. Fiz. **19**, 218 (1974) [Sov. J. Nucl. Phys. **19**, 114 (1974)]; N. H. Buttimore, E. Gotsman, and E. Leader, Phys. Rev. D **18**, 694 (1978); J. Schwinger, Phys. Rev. ; **73**, 407 (1948).

[19] Offline CNI polarization analysis information, document found at http://www4.rcf.bnl.gov/~cnipol/pubdocs/Run09Offline/NOTE_2009_Polarizations_RHIC.txt

[20] Offline CNI yellow beam polarization, document found at http://www4.rcf.bnl.gov/~cnipol/pubdocs/Run09Offline/Pol2009_500gev_yell.dat

[21] Offline CNI blue beam polarization, document found at http://www4.rcf.bnl.gov/~cnipol/pubdocs/Run09Offline/Pol2009_500gev_blue.dat